# ON THE AXIAL ROTATION OF THE BRIGHTER O AND B STARS

ARNE SLETTEBAK
Yerkes Observatory
*Received August 18, 1949*

## ABSTRACT

Rotational velocities have been determined for a total of 123 stars, comprising the brighter O, B2–B5, and B2e–B5e stars. The method involves the comparison of the observed line contours of *He* I 4026 with theoretical line contours computed by means of a graphical method for various equatorial rotational velocities. An attempt has been made to take into account the effects of limb darkening, gravity darkening, and differential rotation on the computed line contours. Values of $v \sin i$ in excess of 400 km/sec were found for several stars in each of the three groups studied.

The Be stars have the most rapid axial rotation observed for any class of stars; their mean rotational velocity was found to be at least 150 km/sec larger than the mean rotational velocity for the corresponding group of B stars. Among the Be stars the shell stars have the largest rotational velocities and the pole-on stars the smallest, which is interpreted as an inclination effect. The observed rotation in the Be stars is somewhat lower than would be expected under the assumption that these stars may be represented by Roche models at the point of rotational instability. It is suggested that radiation pressure and turbulence may be responsible for the discrepancy. Rapid rotation appears to be principally confined to stars on or slightly above the main sequence.

## I. INTRODUCTION

The idea that the axial rotational velocities of the stars could be determined from measurements of the broadening of the spectral lines was first expressed by W. de W. Abney[1] in 1877. Schlesinger,[2] in 1909, obtained the first convincing evidence of axial rotation of stars from the limb effect in the radial-velocity-curve of the eclipsing binary system $\delta$ Librae—an effect which has since been found in many eclipsing systems. Statistical methods by Shajn and Struve[3] in 1929 indicated that, in spectroscopic binaries at least, excessive line broadening is essentially a result of rotation. The extension of this conclusion to single stars is largely due to the investigations of Struve and his co-workers.[4] In 1930 Elvey[5] published the first list of rotational velocities derived from comparisons of measured line contours with contours computed by means of a graphical method suggested by Shajn and Struve.[3] Other lists have followed, the most extensive being that of Miss Westgate.[6] No attempt has been made, however, to derive rotational velocities for those stars which show the broadest and shallowest line contours and which are therefore presumably rotating most rapidly. The existence of very large rotational velocities has been pointed out by Morgan[7] in a low-dispersion study of the spectra of the early B stars; he estimated rotational velocities of 300–400 km/sec for a considerable number of stars, the majority of which are of type Be. It is the object of this investigation, therefore, to derive rotational velocities for the brighter early B and Be stars with the broadest absorption lines, taking into account the effects of limb darkening, gravity darkening, and differential rotation on the rotationally broadened line contours and, further, to compare the B and Be stars with respect to axial rotation.

[1] *M.N.*, **37**, 278, 1877.

[2] *Pub. Allegheny Obs.*, **1**, 134, 1909.

[3] *M.N.*, **89**, 222, 1929.

[4] For a general discussion of the observational evidence for stellar rotation and summary of work in the field to 1945 see Struve, "The Cosmogonical Significance of Stellar Rotation," *Pop. Astr.*, **53**, 201, 259, 1945.

[5] *Ap. J.*, **71**, 221, 1930.

[6] *Ap. J.*, **77**, 141, 1933; **78**, 46, 1933; **79**, 357, 1934.

[7] *A.J.*, **51**, 21, 1944.

## II. THE OBSERVATIONAL MATERIAL

Rotational velocities have been determined for a total of 123 stars, which are divided into the following three groups:

1. All Be stars brighter than magnitude 6.0, north of declination $-30°$, and with spectral types between B2e and B5e on the Morgan-Keenan-Kellman system. Stars of type cBe have not been included, as their emission characteristics are not associated with rapid axial rotation. Group (1) comprises 50 stars.

2. The broadest-lined stars with spectral types between B2 and B5 on the MKK system, brighter than magnitude 5.5, and north of declination $-30°$. The selection in this case was made possible by the classification of all the bright B stars into classes of approximate line width, determined visually by Morgan with low-dispersion spectra. A total of 52 stars was studied.

3. All stars of spectral types O5–O9, brighter than magnitude 6.0, and north of declination $-30°$. This group contains 21 stars.

In all three groups, systems showing two spectra were eliminated.

The spectra were obtained with a small one-prism spectrograph attached to the 40-inch telescope of the Yerkes Observatory and were greatly widened to reduce the effects of plate grain on the microphotometer tracings. The dispersion is approximately 60 A/mm at $H\gamma$ and 40 A/mm at $\lambda$ 4026. Eastman 103*a*-O plates were used and developed in a fine-grain developer similar to Kodak D-23. Calibration of the plates was effected by means of a step-slit spectral sensitometer, which, in turn, was calibrated photoelectrically at $\lambda$ 4026. The line contours were finally obtained from microphotometer tracings made with the Beals microphotometer of the Yerkes Observatory.

## III. THE METHOD OF DETERMINING THE ROTATIONAL VELOCITIES

The graphical method suggested by Shajn and Struve[3] and first employed by Elvey[5] was used to determine the rotational velocities. The idea underlying this method is to assume that the undisturbed contour of a line is similar to that actually observed in a narrow-lined star of similar spectral class—an assumption which has been justified by the work of Carroll.[8] The apparent disk of the star is divided into a number of strips parallel to the axis of rotation, each producing the contour of the narrow-lined star multiplied by a factor such that the equivalent width is proportional to the relative area of the strip, for the case of a uniform stellar disk. Any value chosen for the equatorial rotational velocity of the star then determines the radial velocity of each strip and therefore the Doppler shift of the contour produced by that strip. The summation of the contributions from all the strips gives the rotationally broadened contour, which is then fitted to the observed contour to obtain the rotational velocity of the star. In the present work 40 strips were used.

Despite the pronounced Stark effect present in helium, the line *He* I 4026 seemed to be the most suitable and was accordingly used in the determination of the rotational velocities. It has the advantage of reaching maximum intensity at spectral types B2–B3, which means that little change in the line contour is expected in the range of spectral types considered.

Two standard narrow-lined stars have been selected to represent zero rotational velocity: $\iota$ Herculis for the more intense lines and $\epsilon$ Cassiopeiae for the fainter lines.[9] Both are of spectral type B3 and near the main sequence, according to Morgan. The observed line profiles have been scaled to the same equivalent width of one or the other of the sets of rotational profiles derived from the standard stars, so that an accurate comparison can be made. With the spectrograph used, the *He* I 4026 profiles in the standard

[8] *M.N.*, **93**, 478, 508, 680, 1933.

[9] The weakness of the helium lines in $\epsilon$ Cassiopeiae was pointed out by Morgan in *An Atlas of Stellar Spectra* (Chicago: University of Chicago Press, 1943). No explanation is available as yet.

stars are largely instrumental. The $\iota$ Herculis profile shows an asymmetry which seems to be real and was therefore not removed; the violet wing is somewhat stronger than the red. This asymmetry may be due to a blending with the forbidden helium line at $\lambda$ 4025.4. It can be shown[10] that the profile of a line broadened by rotational and instrumental effects can be represented by applying the rotation to the observed, instrumentally broadened line profiles of a nonrotating star. Since the standard line contours from the nonrotating stars were obtained with the same spectrograph and under the same conditions as the line contours from the rotating stars investigated, the effect of instrumental broadening was not taken into account.

Figure 1 illustrates the observed line profiles of *He* I 4026 in $\iota$ Herculis and $\epsilon$ Cassiopeiae, and rotational profiles derived from them for several values of the equatorial rotational velocity, on the assumption of a uniform stellar disk.

## IV. THE EFFECTS OF LIMB DARKENING

The assumption of a uniform stellar disk is a crude one; effects such as limb darkening and, for the most rapidly rotating stars, gravity darkening must play a role, and it is of importance to determine their influence in computing the contours. An attempt has been made to take some of these factors into account, though the results can be considered only as a first approximation. Thus a linear law of darkening (see below) has been assumed and the darkening coefficients computed for the B2–B5 stars and for the O stars; but the variation of the absorption line itself, owing to the dependence of the effective optical depth on the distance from the center of the disk, has been ignored. A decrease in equivalent width from center to limb would be expected,[11] so that the inclusion of this effect would tend to make the computed line contour slightly deeper and narrower and therefore would increase the measured rotational velocities. The amount of increase is probably not more than that due to the limb darkening, however, which amounts to about 4 per cent for the B2–B5 stars and about 8 per cent for the O stars.

The law of darkening for a stellar atmosphere in local thermodynamic equilibrium is given by

$$I_\nu(\theta) = \int_0^\infty B_\nu(T_\tau) \exp\left(-\frac{\kappa_\nu}{\bar{\kappa}}\tau \sec\theta\right) d\left(\frac{\kappa_\nu}{\bar{\kappa}}\tau \sec\theta\right), \tag{1}$$

where $I_\nu(\theta)$ is the emergent intensity in the frequency $\nu$ and in the direction inclined at an angle $\theta$ to the normal, $B_\nu(T_\tau)$ is the Planck intensity in the frequency $\nu$ and at the temperature $T_\tau$ prevailing at the optical depth $\tau$, $\kappa_\nu$ is the monochromatic absorption coefficient, $\bar{\kappa}$ is the mean absorption coefficient weighted with respect to the fluxes, and $\kappa_\nu/\bar{\kappa}$ is assumed to be independent of depth.

In main-sequence and giant stars of spectral types B2–B5, the continuous absorption arises principally from the photoionization of hydrogen and, to a lesser extent, from electron scattering. Aller[12] has computed $\kappa_{\lambda\,4100}$ and $\bar{\kappa}$ as a function of $\tau$ for the main-sequence B2.5 star, $\gamma$ Pegasi. From Aller's tables an average value of unity is found for $\kappa_{\lambda\,4100}/\bar{\kappa}$ for those optical depths in which the *He* I 4026 line is formed. Employing this value in equation (1) and evaluating the latter by means of Chandrasekhar's[13] tables, we obtain $I_{\lambda\,4100}(\theta)/I_{\lambda\,4100}(0)$ as a function of $\theta$. This gives a darkening coefficient $u = 0.35$, if a linear law of darkening,

$$I_{\lambda\,4100}(\theta) = I_{\lambda\,4100}(0)\,[1 - u + u\cos\theta], \tag{2}$$

is assumed.

[10] E. van Dien, "Axial Rotation of the Brighter Pleiades," *J.R.A.S. Canada*, **42**, 249, 1948.

[11] Struve, "The Spectrographic Problem of U Cephei," *Ap. J.*, **99**, 222, 1944.

[12] *Ap. J.* **109**, 244, 1949.

[13] *Ap. J.*, **105**, 461, 1947.

The continuous absorption in the O stars is almost entirely due to electron scattering. Chandrasekhar[14] has obtained the law of darkening for a star in which electron scattering is the sole cause of the continuous opacity; a darkening coefficient of $u = 0.66$ results for all wave lengths.

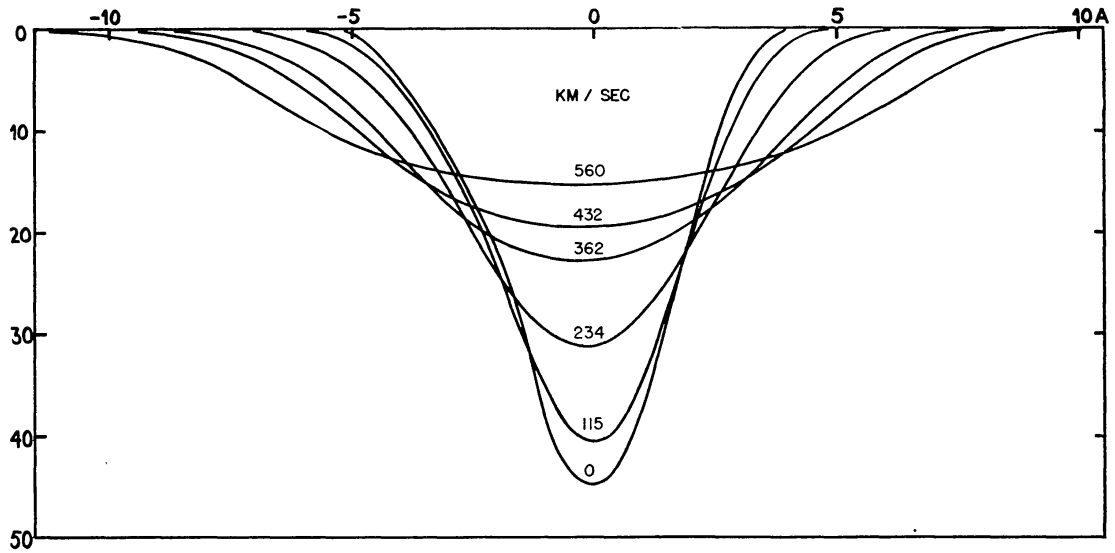


FIG. 1*a*.—The *He* I 4026 line contour observed in $\iota$ Herculis (0 km/sec) and rotational contours derived from it for five values of the equatorial rotational velocity, under the assumption of a spherical, undarkened star. Ordinate is the percentage of absorption.

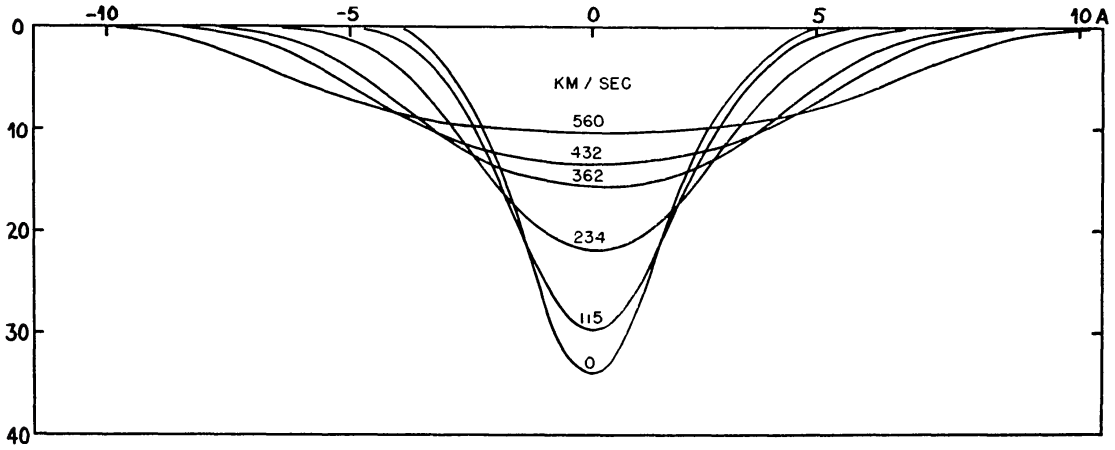


FIG. 1*b*.—The *He* I 4026 line contour observed in $\epsilon$ Cassiopeiae (0 km/sec) and rotational contours derived from it for five values of the equatorial rotational velocity, under the assumption of a spherical, undarkened star. Ordinate same as in Fig. 1*a*.

Figure 2 illustrates the differences in the computed rotational line profiles of $\iota$ Herculis for a darkened and an undarkened spherical star rotating with an equatorial velocity of 560 km/sec.

## V. THE EFFECTS OF GRAVITY DARKENING

It has been shown by von Zeipel[15] that the surface brightness at any point of a star rotating as a rigid body is proportional to the effective gravity at that point; accordingly,

[14] *Ap. J.*, **103**, 351, 1946.

[15] *M.N.*, **84**, 665, 1924.

the temperature at the poles is greater than at the equator. Recent work by Morgan and associates[16] would seem to confirm the effect of increased polar gravity in rotating stars observationally; an examination of low-dispersion spectra of the Be stars indicates that the majority of stars with sharp helium lines show hydrogen lines which are very broad (see Fig. 3). Since the Be stars as a class will be shown to have very large rotational velocities, it is reasonable to suppose that those few with sharp helium lines are also rotating rapidly but are viewed along the axis of rotation; the abnormally broad hydrogen lines are then explained as due to the increased gravity at the poles. Struve[4] has suggested that the range of excitation observed in Maia may similarly be explained by the gravity effect. Observational confirmation for those Be stars in which the equatorial regions are observed (i.e., the Be "shell" stars) is much more difficult to obtain, owing to the tremendous rotational broadening of all lines. Thus it will be seen that the conditions of temperature and surface gravity in the equatorial regions of these stars are such that the K line of *Ca* II might be expected. The rotational velocities in these regions are so great, however, that the resultant line profile would be all but unmeasurable.

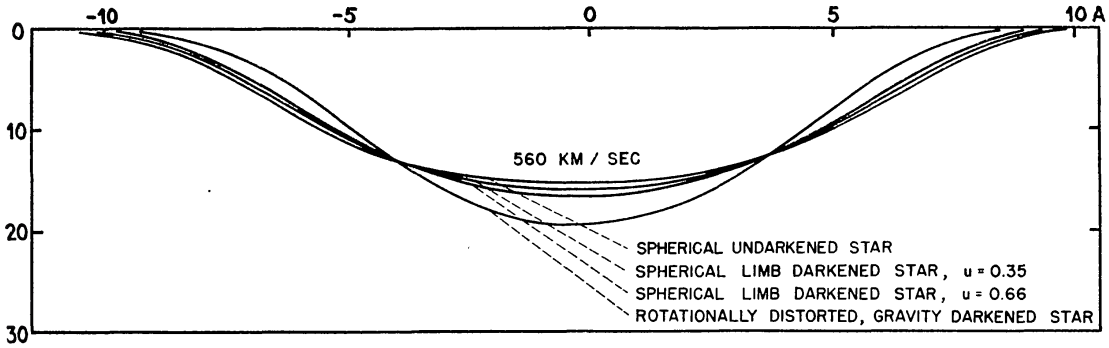


FIG. 2.—The effects of darkening on the *He* I 4026 line contours computed from the observed contour in $\iota$ Herculis for an equatorial velocity of 560 km/sec. Ordinate is the percentage of absorption.

Rotating stars have been considered according to three models: (1) spherical stars, undarkened; (2) spherical stars, limb darkened; and (3) rotationally distorted stars, built on the Roche model, with the surface brightness given by von Zeipel's theorem, but without limb darkening.

For each of these models, profiles of *He* I 4026 were derived for five values of the equatorial velocity specified below. It is obvious that comparison with observed profiles will yield values of $v \sin i$, where $v$ is the equatorial velocity and $i$ the angle between the axis of rotation and the line of sight, for models 1 and 2. This simple relation will not hold for model 3, since, for different values of the inclination $i$, different parts of the stellar surface will contribute to the observed profile. In view of von Zeipel's theorem, these areas will appear with different surface brightness and temperature and consequently different intensity of *He* I 4026. Rotational profiles of *He* I 4026 for model 3 have to be computed with an assumed value of the inclination. Only the case where the axis of rotation is perpendicular to the line of sight has been considered in the following computations, in which case $\sin i = 1$, and the equatorial rotational velocity is obtained directly. In practice, information about $\sin i$ in single stars is available for only two groups of Be stars: the "pole-on" stars, which have already been mentioned, and the "shell" stars. The spectra of the latter are characterized by the simultaneous presence of extremely broad absorption lines of *He* I, indicating very rapid axial rotation, and deep, narrow absorption lines of hydrogen and occasionally of other atoms. Struve[4] attributes the sharp lines to a tenuous shell of material surrounding the rotating star and generally confined to its

[16] Unpublished.

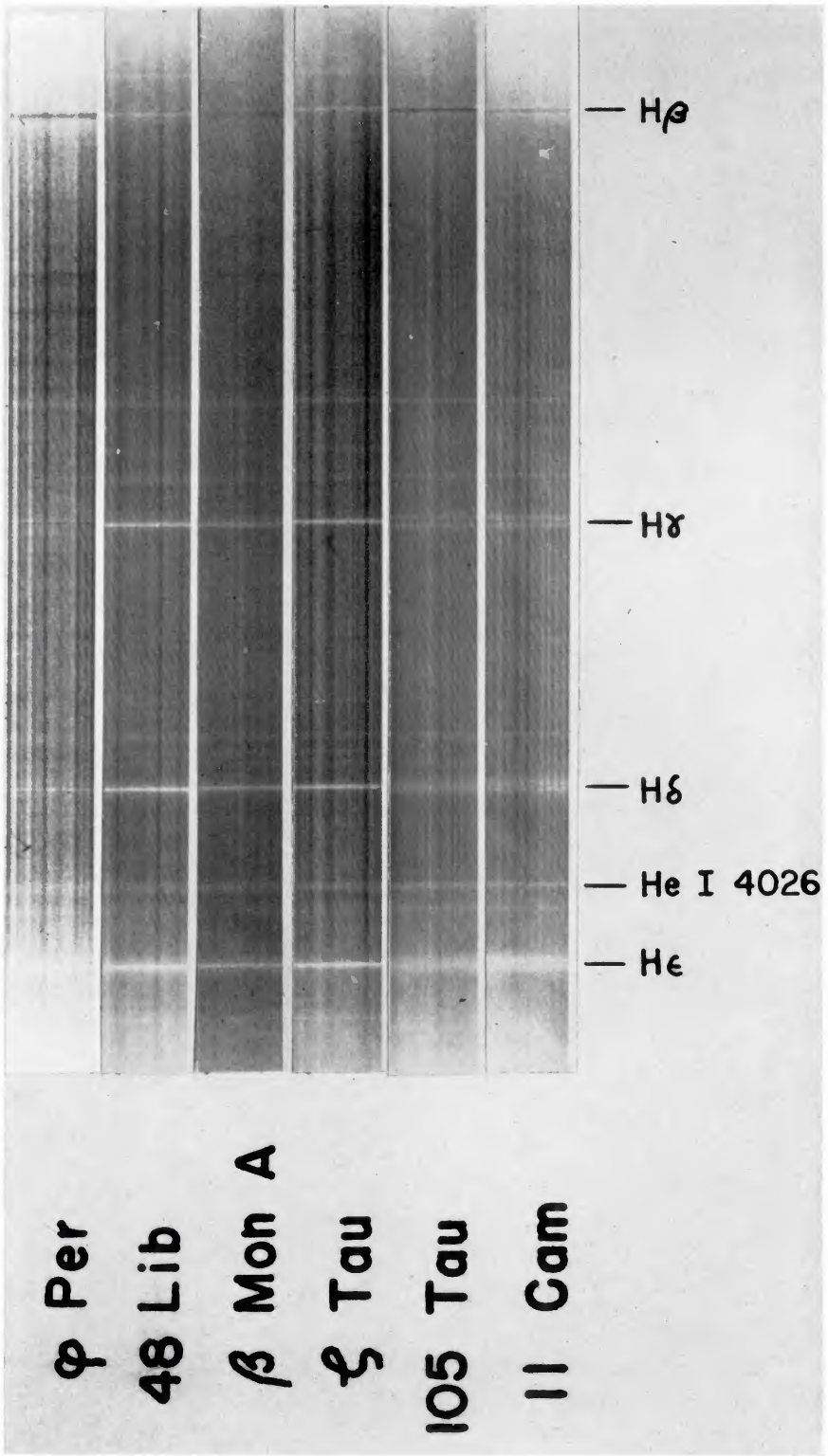


FIG. 3.—Spectra of some Be stars, illustrating inclination effects. The top four spectra are of shell stars; the bottom two of pole-on stars

equatorial plane. The shell is responsible for the observed emission in the Be stars for all values of the inclination but will produce its characteristic sharp absorption lines only when the observer is in the equatorial plane, that is, when $\sin i = 1$. Thus the computed gravity-darkened line contours may be applied directly to the observed line contours of the Be shell-type stars, to obtain the equatorial rotational velocities for these stars.

The computations were carried out under the following assumptions:

1. The star may be represented by a Roche model, in which the total mass is concentrated at a point at the center of the star. Chandrasekhar[17] has shown that the shape of a rotating star computed on the simple Roche model will not differ appreciably from that computed for stars which are polytropes of index $n = 3.5$ or 4, as seems to be the case for ordinary stars.[18] This result is a consequence of the fact that some 90 per cent of the mass is located within less than half the radius from the center, in which region the equipotential surfaces are nearly spheres; hence the attraction on an exterior point is very nearly the same as that valid for the Roche model.

2. The volume (or, equivalently, the mean density, since there is no change in mass) and the luminosity of the star remain constant for all values of the rotational velocity. Actually, a more direct assumption would be that the mean effective gravity and the mean temperature do not change in the sequence of rotational velocities considered. The observational selection has been by spectrum, and the standard nonrotating stars were chosen to be of the same spectral type as the stars under investigation; therefore, the assumption that the spectrum, and hence the mean effective gravity and mean temperature, remain constant with respect to rotation is implicit in the problem. It will be shown, however, that the assumption of constant volume and luminosity is very nearly equivalent and has the advantage of simplifying the calculations considerably.

Jeans[19] has discussed the stability of Roche's model with respect to rapid axial rotation. The potential of a single mass rotating freely in space is

$$\Omega = \frac{GM}{r} + \tfrac{1}{2}\omega^2 (x^2 + y^2) , \tag{3}$$

where $M$ is the mass of the body, $\omega$ is the angular velocity, $r$ is the distance of a point $(x, y, z)$ from the mass center, and $z$ is directed along the axis of rotation. As $\omega$ increases, the model will depart more and more from sphericity, bulging out in the equatorial regions until a point is reached when, at the equator, the centrifugal force is just equal to the gravitational force,

$$\omega_c^2 R_0 = \frac{GM}{R_0^2} , \tag{4}$$

where $R_0$ is the radius of the cross-section in the equatorial plane and $\omega_c$ is the critical angular velocity. At this stage the surface of the rotating configuration is given by

$$\frac{1}{r} + \frac{1}{2}\frac{x^2 + y^2}{R_0^3} = \frac{3}{2}\frac{1}{R_0} . \tag{5}$$

If $\bar{\rho}$ denotes the mean density of all the matter inside this critical equipotential, the relation

$$\frac{\omega_c^2}{2\pi G\bar{\rho}} = 0.3\,6075 \tag{6}$$

may be shown to hold. The critical case is of particular interest, since it appears likely that the Be stars have evolved in the manner just described, leaving rings of material in

[17] *M.N.*, **93**, 539, 1933.

[18] M. Schwarzschild, *Ap. J.*, **104**, 203, 1946; M. Harrison, *Ap. J.*, **108**, 310, 1948.

[19] *Astronomy and Cosmogony* (Cambridge: At the University Press, 1928), p. 243.

the equatorial plane.[4] Employing Kuiper's temperature scale and bolometric corrections,[20] and his empirical mass-luminosity and mass-radius diagrams,[21] we find a mass of 8.0 $\odot$ and a radius of 4.0 $R_\odot$ for the B3 standard nonrotating stars; this results in a mean density of 0.18 gm/cm$^3$. Under the assumption of constant mean density, this value is inserted into equation (6), giving $\omega_c = 1.65 \times 10^{-4}\text{sec}^{-1}$; and, from equation (4), $R_0 = 4.88\ R_\odot$; the resultant equatorial rotational velocity is 560 km/sec. The effective gravity at a point on the critical equipotential surface is given by the derivative of the potential with respect to the normal to the surface at that point and may be obtained as a function of $z$ from equations (3) and (5).

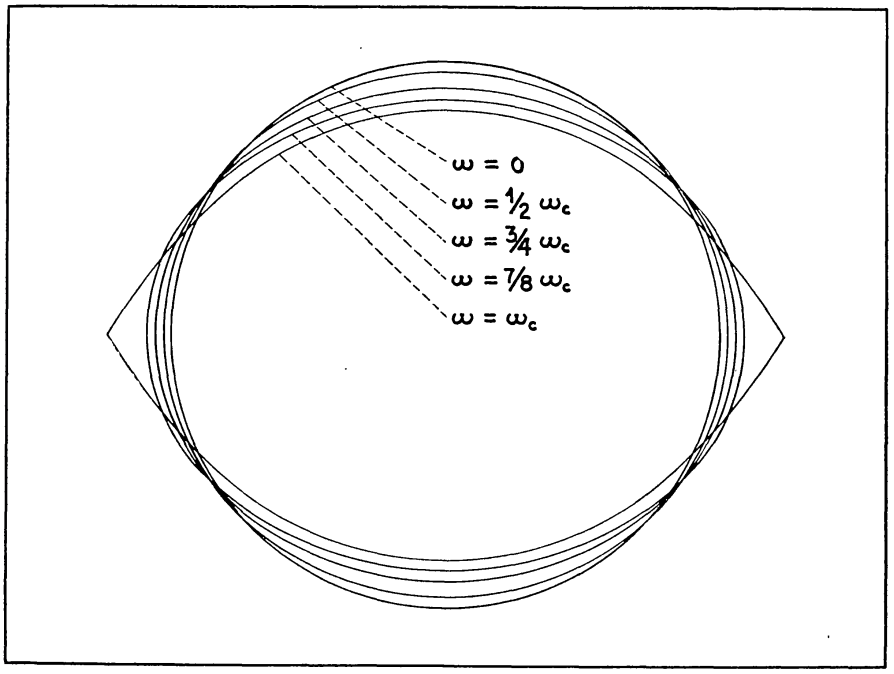


FIG. 4.—Meridional cross-sections of Roche models rotating with various values of the angular velocity $\omega$, under the assumption of constant volume for all angular velocities.

The cases $\omega < \omega_c$ are also of interest; they give an indication of the magnitude of the gravity darkening and the resultant effect on the line profile as a function of the axial rotation. We have considered four values, $\omega = 7/8\omega_c$, $3/4\omega_c$, $1/2\omega_c$, and $1/4\omega_c$, employing the following procedure: The appropriate angular velocity for a particular model is substituted in equation (3), and an arbitrary value of $\Omega$ is specified. This defines an equipotential surface, the volume of which can be determined and compared with the volume of the standard nonrotating star. By trial and error, that value of $\Omega$ is obtained which makes the two volumes equal, and the surface of the rotating configuration is thereby determined. To facilitate the computations, the assumption is made that these surfaces are ellipsoids—an assumption which is not far from the truth for values of $\omega$ even as large as $7/8\omega_c$. The effective gravity is now computed across the stellar surface in the same manner as was done for the model $\omega = \omega_c$. Meridional cross-sections of the five models considered are illustrated in Figure 4.

Now, according to von Zeipel,

$$H \sim g\ , \tag{7}$$

[20] *Ap. J.*, **88**, 446, 1938.

[21] *Ibid.*, p. 472.

where $g$ is the local effective gravity and $H$ the bolometric surface brightness; the latter is related to the effective temperature, $T_e$, by the Stefan-Boltzmann law,

$$H = \sigma T_e^4 . \tag{8}$$

It follows that

$$T_e \sim g^{1/4} ; \tag{9}$$

knowing the effective gravity as a function of $z$ on the surface of the star, we can determine the run of $T_e$ from equator to pole for any model. The proportionality constant inherent in relation (9) follows from the assumption that the luminosity of a rotating configuration is constant for all values of $\omega$ and equal to the luminosity of the standard nonrotating star. The given model is divided into sections by planes parallel to the equator and separated by a distance equal to one-twentieth of the equatorial radius; and the surface areas of the sections thus defined are obtained. If the surface area of the $i$th section

TABLE 1

THE VARIATION OF EFFECTIVE GRAVITY AND EFFECTIVE TEMPERATURE ON THE STELLAR SURFACE

| LATITUDE $\phi$ | $\omega = \omega_c$ (560 Km/Sec) | | $\omega = \frac{7}{8}\omega_c$ (432 Km/Sec) | | $\omega = \frac{3}{4}\omega_c$ (362 Km/Sec) | | $\omega = \frac{1}{2}\omega_c$ (234 Km/Sec) | | $\omega = \frac{1}{4}\omega_c$ (115 Km/Sec) | |
|---|---|---|---|---|---|---|---|---|---|---|
| | log $g_e$ | $T_e$ | log $g_e$ | $T_e$ | log $g_e$ | $T_e$ | log $g_e$ | $T_e$ | log $g_e$ | $T_e$ |
| 1° | 2.50 | 8,190° | 3.76 | 16,390° | 3.90 | 17,320° | 4.06 | 18,370° | 4.12 | 18,670° |
| 3 | 2.95 | 10,850 | 3.77 | 16,510 | 3.90 | 17,320 | 4.06 | 18,370 | 4.12 | 18,670 |
| 6 | 3.23 | 12,750 | 3.78 | 16,580 | 3.91 | 17,440 | 4.06 | 18,370 | 4.12 | 18,670 |
| 10 | 3.45 | 14,470 | 3.80 | 16,770 | 3.92 | 17,520 | 4.06 | 18,370 | 4.13 | 18,800 |
| 20 | 3.76 | 17,280 | 3.88 | 17,560 | 3.96 | 17,930 | 4.07 | 18,500 | 4.13 | 18,800 |
| 30 | 3.93 | 19,080 | 3.98 | 18,605 | 4.02 | 18,570 | 4.08 | 18,580 | 4.13 | 18,800 |
| 40 | 4.07 | 20,670 | 4.07 | 19,610 | 4.08 | 19,210 | 4.10 | 18,800 | 4.14 | 18,880 |
| 50 | 4.17 | 21,900 | 4.15 | 20,530 | 4.14 | 19,890 | 4.12 | 19,030 | 4.14 | 18,880 |
| 60 | 4.23 | 22,680 | 4.20 | 21,120 | 4.18 | 20,350 | 4.14 | 19,240 | 4.15 | 19,010 |
| 70 | 4.28 | 23,310 | 4.25 | 21,760 | 4.21 | 20,740 | 4.16 | 19,450 | 4.15 | 19,010 |
| 80 | 4.31 | 23,750 | 4.27 | 22,020 | 4.23 | 20,970 | 4.17 | 19,600 | 4.15 | 19,010 |
| 90 | 4.32 | 23,850 | 4.28 | 22,110 | 4.24 | 21,070 | 4.18 | 19,690 | 4.15 | 19,010 |

is designated by $A_i$ and the effective temperature of this section is $T_i$, then the luminosity of the model rotating with angular velocity $\omega$ is given by

$$L_\omega = \sigma \sum_i A_i T_i^4 . \tag{10}$$

Now, according to relation (9),

$$T_i^4 = c\, g_i , \tag{11}$$

where $g_i$ is the effective surface gravity at the midpoint of the $i$th section and $c$ is a constant. From equations (10) and (11) and the constant-luminosity assumption,

$$L_\omega = c\sigma \sum_i A_i g_i = L_{\omega=0} , \tag{12}$$

and therefore,

$$c = \frac{L_{\omega=0}}{\sigma} \sum_i A_i g_i . \tag{13}$$

The run of effective gravity and effective temperature on the stellar surface is given in Table 1 for the five models under consideration.

A mean effective gravity and effective temperature can be found for each model and can be compared with the gravity and effective temperature assumed for the standard nonrotating star; the model $\omega = \omega_c$ shows the greatest differences: 6 per cent in the mean effective gravity and 1.5 per cent in the weighted mean effective temperature, $\sqrt[4]{\overline{T_e^4}}$. The assumptions of constant volume and luminosity are therefore nearly equivalent to the assumptions of constant gravity and temperature.

The effect of the variation of the effective gravity and effective temperature, for any particular model, on the rotational line profile of *He* I 4026 can now be determined. To do this, it is convenient to divide the star, as seen from a point in the plane of its equator, into squares, the sides of which are one-twentieth the length of the equatorial radius. The intensity of the *He* I 4026 line produced by any one such square is obtained and multiplied by the intensity of the neighboring continuous spectrum. The contributions from the squares making up one strip parallel to the axis of rotation are then summed to give the weight factor for that strip, and the graphical method already discussed is employed to obtain the rotational contour.

The intensity of the continuous spectrum near λ 4026 is considered first. The Planck intensity at this wave length, and within the range of temperatures centered around 18,880° considered, can be represented by

$$I_{\lambda\,4026} = cT^p \,. \tag{14}$$

The exponent $p$ is then obtained by taking the derivative of the log of the Planck function with respect to the log of the temperature and substituting the appropriate values; it is found to have a value very close to 2. Using relations (7) and (8), it follows that

$$I_{\lambda\,4026} \sim g^{1/2} \,, \tag{15}$$

which permits the computation of $I_{\lambda\,4026}$ across the stellar surface.

To obtain approximate values of the variation of the intensity of *He* I 4026 with gravity and temperature, we have employed the computations of Pannekoek[22] for *He* I 4471. Since the two lines result from successive transitions in the $2^3P-n^3D$ series of *He* I, their dependence on $g$ and $T$ must be quite similar. Variations in the shape of the line contour due to Stark effect have not been taken into account.

With the weights for the various strips known, the rotational profiles were computed as described, one set being derived from the *He* I 4026 profile of each of the two standard nonrotating stars. Within each set the line contours were again normalized to the same equivalent width. The gravity-darkened line contour corresponding to the critical angular velocity $\omega_c$ and obtained from the $\iota$ Herculis standard contour is illustrated in Figure 2. The difference between the gravity-darkened and the limb-darkened contours for this case is seen to be quite large. However, the importance of the gravity effect falls off very rapidly with decreasing axial rotation: at $7/8\omega_c$, the gravity-darkened contour is almost identical with the limb-darkened contour for $u = 0.35$, and at $3/4\omega_c$ it is already indistinguishable from the undarkened contour.

## VI. THE EFFECTS OF DIFFERENTIAL ROTATION

Differential rotation, like the other effects discussed, will tend to make the computed rotational line contours deeper and narrower and therefore will increase the rotational velocities derived. Since no observational data are available on differential rotation in stars other than the sun, we have estimated the order of magnitude of the effect on rotational line profiles by assuming the law of differential rotation operating in the sun and scaling it up to the rotational velocities found in the early-type stars. The extrapolation is a large one and would probably lead to great shearing forces in a star rotating with an

[22] "The Theoretical Intensities of Stellar Absorption Lines," *Amsterdam Pub.*, No. 4, 1935.

equatorial velocity of several hundred km/sec. The law of differential rotation was obtained from Adams'[23] spectroscopic measurements of the solar rotation, based on the *Ca* I 4227 line and the reversing layer. Again the rotational profile was determined numerically with the aid of the graphical method previously described. The computation was carried out for a spherical, undarkened star only, rotating with an equatorial velocity of 560 km/sec. Figure 5 shows the rotational profile thus obtained and compares it with the profile derived from a spherical, undarkened star rotating as a rigid body with the same equatorial velocity. It appears that the effect on the profile is small, and, because of the many uncertainties involved, no use has been made of differential rotation profiles in obtaining rotational velocities.

## VII. RESULTS AND DISCUSSION

1. Tables 2, 3, and 4 list the values of $v \sin i$ derived for the three groups of stars investigated. The writer has determined the spectral types on the MKK system for the B and Be stars, while the spectral types for the O stars used are due to Plaskett and

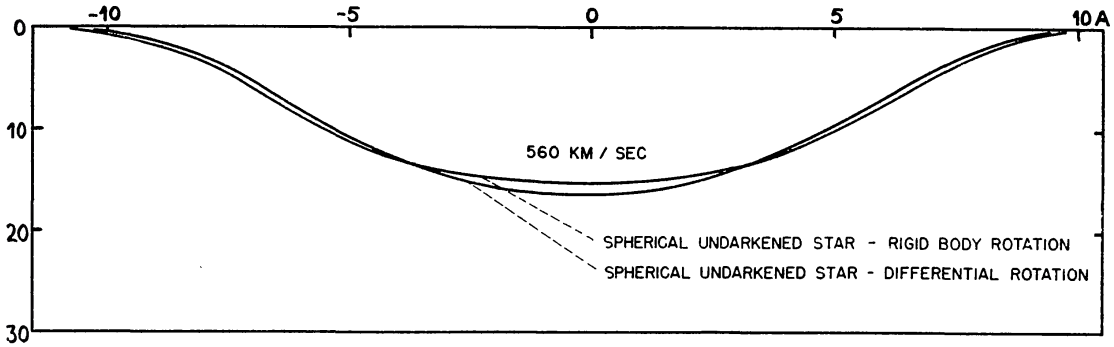


FIG. 5.—The effect of differential rotation on the *He* I 4026 line contours computed from the observed contour in $\iota$ Herculis for an equatorial rotational velocity of 560 km/sec. Ordinate is the percentage of absorption.

Pearce.[24] The observed contours of all the B and Be stars, with the exception of the shell star, $\phi$ Persei, were fitted to contours computed for a spherical star with limb darkening, $u = 0.35$. The rotational velocity for $\phi$ Persei was obtained by comparison with the gravity-darkened contour corresponding to the critical angular velocity. For the O stars, contours were employed under the assumption of a spherical star with limb darkening, $u = 0.66$. The equivalent width of *He* I 4026 in a number of stars fell about halfway between the values measured in $\epsilon$ Cassiopeiae and $\iota$ Herculis; for these cases rotational velocities were obtained from both sets of computed contours, and the agreement was found to be good. The values of $v \sin i$ are given in the tables to the nearest 10 km/sec; this is not intended to indicate the accuracy of an average determination. Given a symmetrical observed line contour, it is possible to distinguish steps of 10 km/sec in $v \sin i$ by the graphical method. However, asymmetrical line contours, with a resulting decrease in accuracy, were obtained for approximately one-third of the stars investigated. In the tables a colon following a rotational velocity indicates a serious asymmetry, causing an estimated uncertainty of 40–70 km/sec in $v \sin i$. All rotational velocities below about 120 km/sec are also uncertain, since, as Figure 1 indicates, the difference between the zero and 115 km/sec rotational contours is quite small. Finally, the results obtained for the O stars give only orders of magnitude; there is no reason to believe that the $\lambda$ 4026 contour in the O stars, which will, in general, be due to both *He* I and *He* II, should be similar to the *He* I 4026 contour observed in B3 stars. This line is also quite weak in some

[23] *Ap. J.*, 29, 136, 1909.

[24] *Pub. Dom. Ap. Obs. Victoria*, 5, 99, 1931.

TABLE 2

B2e–B5e STARS

| Star | MWC | $\alpha$ (1900) | $\delta$ (1900) | $m$ | Sp. | $v \sin i$ (Km/Sec) | Remarks |
|---|---|---|---|---|---|---|---|
| o Cas | 8 | $0^h39^m.2$ | +47° 44′ | 4.70 | B3 | 270 | |
| $\phi$ Per | 16 | 1 37.4 | +50 11 | 4.19 | B2 | 560 | Shell star |
| HD 20336 | 65 | 3 11.2 | +65 17 | 4.76 | B3 | 340 | |
| $\psi$ Per | 69 | 3 29.4 | +47 52 | 4.26 | B5 | 420 | |
| HD 22780 | 463 | 3 34.6 | +37 15 | 5.57 | B5–8 | 360 | |
| 17 Tau | 72 | 3 38.9 | +23 48 | 3.81 | B5–8 | 270: | |
| 23 Tau | 73 | 3 40.4 | +23 38 | 4.25 | B5–8 | 300 | |
| 48 Per | 81 | 4 01.4 | +47 27 | 4.03 | B3 | 230 | Pole-on star* |
| HD 28497 | 86 | 4 24.5 | −13 16 | 5.50 | B2 | 340 | |
| 56 Eri | 89 | 4 39.3 | − 8 41 | 5.87 | B2 | 240 | Pole-on star |
| 11 Cam | 96 | 4 57.5 | +58 50 | 5.31 | B3 | 120 | Pole-on star |
| 105 Tau | 98 | 5 02.0 | +21 34 | 5.95 | B2 | 220 | Pole-on star |
| 25 Ori | 110 | 5 19.6 | + 1 45 | 4.73 | B2 | 320 | |
| 120 Tau | 111 | 5 27.7 | +18 28 | 5.50 | B2 | 280 | |
| $\zeta$ Tau | 115 | 5 31.7 | +21 05 | 3.00 | B3 | 310 | Shell star |
| $\omega$ Ori | 117 | 5 33.9 | + 4 04 | 4.54 | B2 | 190 | |
| HD 41335 | 133 | 5 59.4 | − 6 42 | 5.12 | B2 | 380 | |
| HD 43285 | 136 | 6 10.3 | + 6 06 | 5.95 | B5 | 290 | |
| HD 44458 | 138 | 6 16.8 | −11 44 | 5.49 | B2 | 270 | |
| $\nu$ Gem | 141 | 6 23.0 | +20 17 | 4.06 | B5–8 | 220 | |
| $\beta$ Mon A | 143 | 6 24.0 | − 6 58 | 4.73 | B3 | 420 | Shell star |
| HD 45995 | 146 | 6 25.6 | +11 19 | 5.83 | B2 | 320 | |
| HD 54309 | 167 | 7 03.2 | −23 41 | 5.75 | B2 | 290 | |
| 27 CMa | 170 | 7 10.2 | −26 11 | 4.66 | B2 | 200 | |
| $\omega$ CMa | 171 | 7 10.8 | −26 36 | 3.83 | B3 | 90: | Pole-on star |
| HD 58343 | 177 | 7 20.2 | −16 00 | 5.20 | B3 | 30: | Pole-on star |
| HD 60855 | 565 | 7 31.5 | −14 16 | 5.57 | B3 | 240 | |
| HD 83953 | 197 | 9 36.7 | −23 08 | 4.74 | B5 | 330 | |
| $\kappa$ Dra | 222 | 12 29.2 | +70 20 | 3.88 | B5–8 | 280 | |
| $\theta$ CrB | 237 | 15 28.9 | +31 42 | 4.17 | B5 | 400 | |
| 48 Lib | 239 | 15 52.9 | −13 59 | 4.68 | B5 | 400 | Shell star |
| $\chi$ Oph | 241 | 16 21.2 | −18 14 | 4.85 | B2 | 100: | Pole-on star |
| HD 168797 | 601 | 18 16.6 | + 5 24 | 6.04 | B3 | 300 | |
| HD 171780 | 604 | 18 31.5 | +34 22 | 5.93 | B5 | 310 | |
| HD 174237 | 608 | 18 44.5 | +52 53 | 5.76 | B3 | 170 | |
| HD 178175 | 311 | 19 02.4 | −19 27 | 5.41 | B2 | 220 | |
| 12 Vul | 323 | 19 46.8 | +22 21 | 4.91 | B5 | 300 | |
| 25 Cyg | 624 | 19 56.3 | +36 46 | 5.15 | B3 | 230 | |
| 28 Cyg | 329 | 20 05.7 | +36 33 | 4.82 | B3 | 310 | |
| 60 Cyg | 360 | 20 57.7 | +45 46 | 5.24 | B2 | 320: | |
| $\upsilon$ Cyg | 364 | 21 13.8 | +34 29 | 4.42 | B2 | 280 | Pole-on star |
| $\epsilon$ Cap | 373 | 21 31.5 | −19 55 | 4.72 | B3 | 280 | |
| 16 Peg | 644 | 21 48.5 | +25 27 | 5.05 | B3 | 150 | |
| HD 208682 | 381 | 21 52.9 | +64 51 | 5.85 | B2 | 350: | |
| HD 209522 | 650 | 21 58.9 | −27 18 | 5.84 | B5 | 300 | |
| 31 Peg | 387 | 22 16.6 | +11 42 | 4.93 | B2 | 130 | |
| 8 Lac br | 390 | 22 31.4 | +39 07 | 5.83 | B2 | 360 | |
| HD 217050 | 394 | 22 52.7 | +48 09 | 5.20 | B5 | 380: | Shell star |
| o And | ..... | 22 57.3 | +41 47 | 3.63 | B5–8 | 360 | Shell star |
| $\beta$ Psc | 396 | 22 58.8 | + 3 17 | 4.58 | B5–8 | 160 | Pole-on star |

* For meaning of term "pole-on star" see text above.

TABLE 3

B2–B5 STARS

| Star | $\alpha$ (1900) | $\delta$ (1900) | $m$ | Sp. | $v \sin i$ (Km/Sec) |
|---|---|---|---|---|---|
| HD 1976 | $0^h18^m.9$ | +51° 28′ | 5.36 | B3 | 230 |
| $\pi$ And | 0 31.5 | +33 10 | 4.44 | B3 | 250 |
| $\xi$ Cas | 0 36.5 | +49 58 | 4.85 | B3 | 230 |
| 31 Per | 3 12.0 | +49 44 | 5.08 | B5 | 320 |
| HD 20809 | 3 16.1 | +48 51 | 5.30 | B5 | 250 |
| 34 Per | 3 22.2 | +49 10 | 4.67 | B3 | 190 |
| $\delta$ Per | 3 35.8 | +47 28 | 3.10 | B5 | 290 |
| HD 24504 | 3 48.8 | +47 35 | 5.34 | B5 | 300 |
| HD 24640 | 3 50.0 | +34 47 | 5.48 | B2 | 130 |
| 35 Eri | 3 56.5 | − 1 50 | 5.25 | B5 | 190 |
| HD 26356 | 4 05.0 | +83 34 | 5.39 | B3 | 320: |
| 72 Tau | 4 21.3 | +22 46 | 5.41 | B5–8 | 230 |
| 49 Eri | 4 32.1 | + 0 48 | 5.32 | B5–8 | 140 |
| $\tau$ Tau | 4 36.3 | +22 46 | 4.33 | B3 | 220 |
| $\lambda$ Eri | 5 04.4 | − 8 53 | 4.34 | B2 | 350 |
| $\rho$ Aur | 5 14.7 | +41 42 | 5.12 | B5 | 90: |
| 23 Ori br | 5 17.6 | + 3 27 | 4.99 | B2 | 280 |
| 115 Tau | 5 21.3 | +17 53 | 5.31 | B3 | 160 |
| 32 Ori | 5 25.4 | + 5 52 | 4.32 | B5 | 190 |
| $\xi$ Ori | 6 06.3 | +14 14 | 4.35 | B3 | 230 |
| 69 Ori | 6 06.3 | +16 09 | 4.92 | B5 | 310 |
| HD 46487 | 6 28.6 | − 1 09 | 5.02 | B5 | 310 |
| HD 49662 | 6 44.4 | −15 02 | 5.29 | B5 | 160 |
| 19 Mon | 6 58.0 | − 4 06 | 4.89 | B2 | 350 |
| 16 Pup | 8 04.6 | −18 57 | 4.34 | B5 | 190 |
| $\kappa$ Hya | 9 35.5 | −13 53 | 4.96 | B5 | 180 |
| $\eta$ UMa | 13 43.6 | +49 49 | 1.91 | B3 | 230 |
| 1 Sco | 15 45.0 | −25 27 | 4.77 | B3 | 340 |
| $\lambda$ Lib | 15 47.5 | −19 52 | 5.06 | B3 | 220 |
| 2 Sco | 15 47.6 | −25 02 | 4.66 | B3 | 310 |
| HD 142165 | 15 47.9 | −24 14 | 5.44 | B5–8 | 290 |
| HD 142184 | 15 48.0 | −23 41 | 5.36 | B3 | 400: |
| $\rho$ Sco | 15 50.7 | −28 55 | 4.02 | B2 | 180 |
| 13 Sco | 16 06.2 | −27 40 | 4.70 | B3 | 210 |
| $\nu$ Sco br | 16 06.2 | −19 12 | 4.29 | B2 | 210 |
| $\rho$ Oph br | 16 19.6 | −23 13 | 5.22 | B2 | 310: |
| 22 Sco | 16 24.1 | −24 54 | 4.87 | B3 | 240 |
| 96 Her | 17 58.1 | +20 50 | 5.09 | B5 | 220 |
| $\sigma$ Sgr | 18 49.1 | −26 25 | 2.14 | B3 | 230 |
| HD 176162 | 18 53.8 | −12 59 | 5.36 | B5 | 190 |
| HD 176871 | 18 57.2 | +26 09 | 5.50 | B5 | 300 |
| $\iota$ Lyr | 19 03.7 | +37 57 | 5.13 | B5–8 | 310: |
| 20 Aql | 19 07.3 | − 8 06 | 5.37 | B5 | 170 |
| 1 Vul | 19 11.9 | +21 13 | 4.60 | B5 | 130 |
| $\iota$ Aql | 19 31.6 | − 1 31 | 4.28 | B5–8 | 120 |
| 23 Cyg | 19 51.2 | +57 16 | 5.04 | B5 | 150 |
| 22 Cyg | 19 52.3 | +38 13 | 4.87 | B5 | 120 |
| 17 Vul | 20 02.6 | +23 20 | 5.08 | B3 | 240: |
| $\tau$ Cap | 20 33.7 | −15 18 | 5.30 | B5–8 | 180 |
| 28 Vul | 20 34.2 | +23 46 | 5.04 | B5 | 330 |
| 7 Cep | 21 25.8 | +66 22 | 5.42 | B5–8 | 300: |
| $\psi^2$ Aqr | 23 12.7 | − 9 44 | 4.56 | B5 | 350 |
| $\sigma$ Cas | 23 53.9 | +55 12 | 4.93 | B2 | 210 |

O stars and consequently difficult to measure accurately. Further, the absorption-line contours of some of the O stars suggest that turbulence must also play a role in the line broadening. There can be no question about the rotational nature of the absorption lines in such stars as $\zeta$ Ophiuchi, $\lambda$ Cephei, and HD 206267, however; and, for stars with such rapid axial rotation, the form of the standard zero-velocity contour employed in the graphical method becomes of secondary importance.

2. Despite the relatively small number of stars which have been investigated, it was thought worth while to plot frequency diagrams for the B and Be stars and see what information could be derived from them; these are reproduced in Figure 6. The frequency

TABLE 4

O-TYPE STARS

| Star | $\alpha$ (1900) | $\delta$ (1900) | $m$ | Sp. | $v \sin i$ (Km/Sec) | Notes |
|---|---|---|---|---|---|---|
| $\xi$ Per | $3^h52^m.5$ | +35° 30′ | 4.05 | O7n | 240 | |
| $\alpha$ Cam | 4 44.1 | +66 10 | 4.38 | O9se | 0 | |
| HD 34078 | 5 09.7 | +34 12 | 5.8 | O9ss | 0 | |
| $\lambda$ Ori br | 5 29.6 | + 9 52 | 3.66 | O8s | 0 | |
| $\theta^1$ Ori C | 5 30.4 | − 5 27 | 5.36 | O7 | 150 | |
| $\theta^2$ Ori br | 5 30.5 | − 5 29 | 5.17 | O9 | 220 | |
| $\iota$ Ori br | 5 30.5 | − 5 59 | 2.87 | O8s | 140 | |
| 15 Mon | 6 35.5 | + 9 59 | 4.68 | O7s | 180: | |
| HD 55879 | 7 09.7 | −10 08 | 5.99 | O9s | 0 | |
| $\tau$ CMa | 7 14.6 | −24 46 | 4.40 | O8 | 180: | |
| $\zeta$ Oph | 16 31.7 | −10 22 | 2.70 | O9.5 | 450 | 1 |
| 9 Sgr | 17 57.8 | −24 22 | 5.86 | O5 | 210 | |
| HD 188209 | 19 49.0 | +46 46 | 5.51 | O8s | 120: | |
| HD 193322 | 20 14.6 | +40 25 | 5.82 | O8 | 200: | |
| HD 199579 | 20 53.1 | +44 33 | 6.01 | O6 | 170 | |
| 68 Cyg br | 21 14.7 | +43 31 | 5.06 | O8nn | 390 | |
| HD 206267 | 21 35.9 | +57 02 | 5.64 | O6n | 490: | 2 |
| HD 207198 | 21 42.1 | +62 00 | 5.97 | O9s | 80: | |
| 19 Cep | 22 02.1 | +61 48 | 5.17 | O9 | 0 | |
| $\lambda$ Cep | 22 08.1 | +58 55 | 5.19 | O6f | 390 | 3 |
| 10 Lac | 22 34.8 | +38 32 | 4.91 | O9s | 0 | |

NOTES TO TABLE 4

1. Spectral type due to Morgan.
2. The very large rotational velocity obtained for this star may be due to the presence of two spectra.
3. Of star.

diagram for the Be stars is complete; that for the B stars lacks 63 stars which were judged to have small rotational velocities from an inspection of low-dispersion plates.

A plot of $v \sin i$ versus galactic latitude for the Be stars shows no particular correlation; it therefore appears safe to assume that the axes of rotation are distributed at random. The question then arises as to whether the same true rotation can be assumed for all the Be stars and the observed frequency curve explained by the random distribution of the axes. The expected frequency distribution[25] under this assumption is given by

$$W(v) = \frac{c}{v_0}\left[\frac{v}{(v_0^2 - v^2)^{1/2}}\right], \tag{16}$$

where

$$v = v_0 \sin i ,$$

[25] For derivation see Struve's paper, *Pop. Astr.*, **53**, 214, 1945.

and $v_0$ is the constant rotational velocity. This distribution has a pronounced maximum at $v_0$, however, and therefore will not represent the observed distribution. Another possible assumption is that all rotational velocities are equally probable. This assumption plus the assumption of random distribution of the axes of rotation can be shown to give rise to a distribution function[26] in $v \sin i$ of the type

$$\psi\,(v \sin i) = c \arccos \frac{v \sin i}{k}, \tag{17}$$

where $k$ is the largest value of $v \sin i$ observed. This frequency-curve is maximum at zero $v \sin i$ and decreases monotonically to zero at $k$; it will also not represent the observed curve. It is possible to obtain a rough idea of the true rotational-velocity distribution, which must lie somewhere between the above extremes, by analyzing the observed dis-

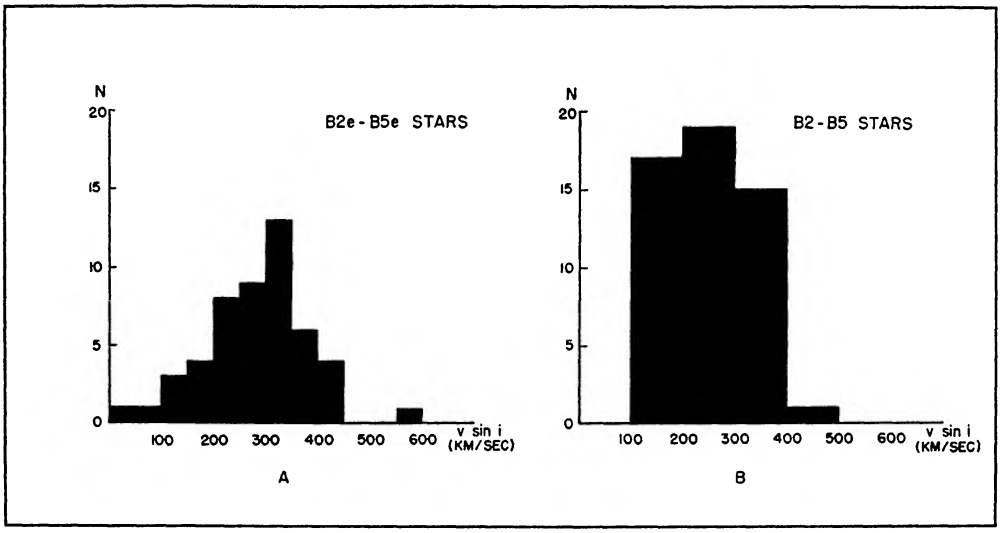


FIG. 6.—The frequencies of observed rotational velocities for the B2e–B5e and B2–B5 stars. Blocks of 50 km/sec are employed in diagram *A*, while diagram *B* illustrates 100 km/sec blocks because of the incompleteness of the data for the B2–B5 stars.

tribution in terms of functions of the type (16). That is, the rotational velocities are assumed to be "quantized" in 50 km/sec steps and the approximate percentage of Be stars in each group found. Omitting $\phi$ Persei from the observed distribution-curve, we obtain the best fit for the distribution of rotational velocities given in Table 5.

The lack of rotational velocities smaller than about 200 or 250 km/sec among the Be stars seems to be real; if even a small percentage of stars is assigned to the lower rotational velocities, it is impossible to obtain a fit at the high-velocity end of the distribution.

The B stars present quite a different picture. The distribution illustrated in Figure 6*B*, is incomplete, as has been mentioned; 63 stars with relatively narrow absorption lines and in the same spectral interval have not been measured and also belong in the diagram. Of these, the majority would probably fall in the 0–100 km/sec block, and most of the others in the 100–200 km/sec block; very few should have values of $v \sin i$ greater than 200 km/sec. The complete frequency distribution would then have a maximum in the 0–100 km/sec or in the 100–200 km/sec range; in either case the mean rotational velocity for the B2–B5 stars must be at least 150 km/sec less than the mean rotational velocity for the B2e–B5e stars.

[26] This distribution function is due to Kuiper, who developed it in investigating a similar problem (see *Pub. A.S.P.*, **47**, 15, 1935).

Table 4 indicates that large rotational velocities are found in individual O stars from spectral types O5–O9.5. A comparision of the group as a whole with the B or Be stars is difficult, owing to the small sample considered; but it can be stated with some certainty that, on the average, the O stars are rotating appreciably less rapidly than the Be stars.

3. Table 2 lists six shell-type stars. One of these, *o* Andromedae, has not been previously announced as either a shell star or of type Be. Both characteristics were discovered by Morgan (1946) from an inspection of Yerkes and McDonald spectrograms. The spectrum shows bright *Hα* and the sharp hydrogen cores characteristic of shell stars. Two other "part-time" shell stars are included in the table but are not designated as "shells": $\epsilon$ Capricorni, which lost its shell spectrum in 1944,[27] and 27 Canis Majoris, which occasionally shows a shell spectrum.[28] The mean observed rotational velocity for the six shell stars listed is 405 km/sec, indicating that, as a class, the shell stars are the most rapidly rotating stars observed. The star $\phi$ Persei is of particular interest; the absorption lines are tremendously broadened (see Fig. 3), resulting in a rotational velocity greater than that obtained for any other star. The observed contour of *He* I 4026 in this star was the only contour measured in any star which was broad and shallow enough to be compared directly with the gravity-darkened contour computed for the critical case, $\omega = \omega_c$, and the rotational velocity obtained, 560 km/sec, rests on this comparison. Even if the comparison is made with the limb-darkened contours, however, the rotational velocity of $\phi$ Persei would still be about 500 km/sec. Axial rotation with this velocity is unusual, even among the Be stars, and for this reason $\phi$ Persei was not included in the above statistical discussion.

TABLE 5

| | | | | | | | | | | |
|---|---|---|---|---|---|---|---|---|---|---|
| $v$ (km/sec)..... | 0 | 50 | 100 | 150 | 200 | 250 | 300 | 350 | 400 | 450 |
| Per cent Be..... | 0 | 0 | 0 | 0 | 0 | 4 | 13 | 36 | 29 | 18 |

It is notable that a direct comparison of the observed line contour with the contour computed for the gravity-darkened critical $\omega_c$ is possible for only one of the six shell stars. If the rotational-instability hypothesis is true for the Be stars, the observed contours for all the shell stars considered would be expected to resemble the computed contour for the critical case, assuming that they are located at approximately the same place in the Hertzsprung-Russell diagram. However, spectroscopic absolute magnitudes are extremely difficult to obtain for the shell stars because of the tremendous broadening of the lines, and it is possible that a considerable dispersion in absolute magnitude exists ($\zeta$ Tauri, in fact, may be of intermediate luminosity). The broadening of the computed line contour is largely determined by the assumed equatorial rotational velocity, which, by an application of Kepler's third law, is proportional to $\sqrt{M/R}$ for the critical case at which instability sets in. If the shell stars which do not fit the computed line contour have a different value of $\sqrt{M/R}$ than that assumed for $\iota$ Herculis, the poor fit may be explained. However, differences in luminosity are not sufficient: to obtain a breakup velocity of approximately 400 km/sec requires that $R \sim M$, which is not quite realized for the main sequence (for which $R \sim M^{3/4}$)[29] and less so for giants. It has been shown that limb darkening and differential rotation will tend to make the computed contours narrower and deeper; the question arises as to whether the superposition of these effects on the gravity darkening for the critical case will result in a better fit with the obesrved contours from the shell stars. The effects are small, and it seems unlikely that their inclusion

[27] Struve and Deutsch, *Ap. J.*, **100**, 390, 1944.

[28] Struve, *Ap. J.*, **96**, 311, 1942.

[29] Kuiper, *Ap. J.*, **88**, 491, 1938.

will improve the fit. Another possibility is that radiation pressure and turbulence, which have not been taken into account, may reduce the stability of the Be stars and thus lower the critical equatorial rotational velocity. These effects are probably quite important.

The width of the broad hydrogen wings which characterize the nine "pole-on" stars listed in Table 2 varies from star to star. It is largest in 11 Camelopardalis, 105 Tauri, and 56 Eridani and decreases until it is just barely noticeable in $\omega$ Canis Majoris and HD 58343. The rotational velocities derived for these stars do not uniformly increase with decreasing hydrogen width, however, as would be expected from the interpretation of the "pole-on" stars given above. The reason may be that the helium contours are also affected by the increased gravity in the polar regions and therefore yield spurious rotational velocities.

One of the O-type stars investigated, $\lambda$ Cephei, is an Of star. This class of O stars was defined by Plaskett and Pearce[24] as characterized by the presence of emission *N* III 4634, 4640, and *He* II 4686. Since $\lambda$ Cephei is rotating quite rapidly, the possibility arises that all the Of stars may similarly be rapidly rotating and the emission explained as being due to a shell thrown off through rotational instability. Visual estimates of line widths for six other Of stars, from low-dispersion plates obtained by Morgan and his associates, indicate that these stars, as a group, have somewhat broader lines than the average absorption O star. Factors other than rotation may play a part in the line broadening, however, so that no definite conclusions can be drawn.

4. As has already been mentioned, it is quite difficult to obtain spectroscopic absolute magnitudes for the rapidly rotating stars because of the great broadening of their spectral lines; for this reason, no attempt has been made to segregate the stars in Tables 2 and 3 into luminosity classes. It is significant, however, that all the stars listed are either main sequence or slightly above the main sequence, with the exception of three: $\delta$ Persei, 19 Monocerotis, and the shell star, $\zeta$ Tauri, which may be intermediate in luminosity. There is no observable axial rotation in the supergiants. The conclusion is that large rotational velocities are restricted primarily to main-sequence stars and stars slightly above the main sequence, of the types investigated, though fairly rapid rotation is occasionally found in intermediate stars.

5. Plots of $v \sin i$ versus galactic latitude and galactic longitude for the Be and B stars show no correlation, thus confirming similar results obtained by Struve and by Miss Westgate.

6. Since the range of the rotational velocities in the Be stars is essentially a result of the inclination of the axis of rotation and since, as has been shown, an appreciable range in temperature exists from equator to pole on the surface of a rapidly rotating star, its spectral type and color should vary with inclination. Both of these quantities will vary together, however, so that a plot of color excess versus $v \sin i$ for a particular spectral class would not be expected to yield any information. This was found to be actually the case.

## VII. CONCLUSIONS

An attempt has been made to obtain rotational velocities for the rapidly rotating early-type stars, taking into account, in an approximate way, the effects of limb darkening, gravity darkening, and differential rotation. It has been shown that:

1. Equatorial rotational velocities in excess of 400 km/sec are to be found among the O, B, and Be stars.

2. The most rapid axial rotation observed for any class of stars is that of the Be stars. The mean equatorial velocity found for a sample of Be stars is at least 150 km/sec larger than the mean equatorial velocity for a corresponding sample of B stars. Statistics for the O stars are incomplete but would seem to indicate that their mean axial rotation is also decidedly less than that obtained for the Be stars. Further, visual inspection of low-dispersion spectrograms of late B, A, and early F stars shows that rotational line broadening

in these stars does not approach the rotational line broadening observed in the Be stars as a class.

3. Among the Be stars, the shell stars have the largest rotational velocities and are, in fact, the most rapidly rotating stars known. As a group, the six investigated have an average observed rotational velocity of 405 km/sec; and one shell star, $\phi$ Persei, is probably rotating with a velocity in excess of 500 km/sec. Shell stars are assumed to have a preferential inclination ($\sin i = 1$), so that for these stars equatorial rotational velocities are measured directly.

4. An observed rotational velocity corresponding to the computed rotational velocity (under the assumption that the Be stars are at the point of rotational instability) is obtained for only one of the six shell stars. It is suggested that radiation pressure and turbulent motions in the Be stars may be responsible for the discrepancy.

5. The smallest values of $v \sin i$ obtained for the Be stars are those of the "pole-on" stars. This is interpreted as an inclination effect and supports the hypothesis that the gravity effect is important for rapidly rotating stars.

6. Axial rotation in the B and Be stars seems to be confined to stars on the main sequence and slightly above it, although a few rapidly rotating stars of intermediate luminosity were found.

I wish to express my sincere thanks to Dr. W. W. Morgan for suggesting this problem and for his advice throughout the investigation. Grateful acknowledgment is also made to Dr. G. P. Kuiper for invaluable discussions of many of the points considered, and to Dr. O. Struve and Dr. S. Chandrasekhar for helpful advice. I am also indebted to Mr. A. D. Code for assistance in calibrating the spectral sensitometer.